Journal of Hydrology 624 (2023) 129895

Contents lists available at ScienceDirect

Journal of Hydrology

journal homepage: www.elsevier.com/locate/jhydrol

Research papers

500-year reconstruction of Dez River discharge in southwestern Iran from tree rings

S. Sharifazari [a,*], J.G. Palmer [b,c], P.A. Higgins [a], M.P. Rao [d,e,f], F. Johnson [a], C.S.M. Turney [b,g], D. Martín-Benito [h], M.S. Andersen [i]

[a] Water Research Centre, School of Civil and Environmental Engineering, University of New South Wales, Australia
[b] Chronos ^{14}Carbon-Cycle Facility, Mark Wainwright Analytical Centre, University of New South Wales, Australia
[c] School of Biological, Earth and Environmental Sciences, University of New South Wales, NSW 2515, Australia
[d] Centre de Recerca Ecològica i Aplicacions Forestals, Bellatera, Catalonia, Spain
[e] Department of Plant Sciences, University of California Davis, USA
[f] Tree Ring Laboratory, Lamont-Doherty Earth Observatory of Columbia University, USA
[g] Division of the Deputy Vice-Chancellor (Research), University of Technology Sydney, Sydney, New South Wales, Australia
[h] Forest Research Center (CIFOR) INIA-CSIC, Ctra. La Coruña km 7.5, 28040 Madrid, Spain
[i] Water Research Laboratory, School of Civil and Environmental Engineering, University of New South Wales, Australia

ARTICLE INFO

This manuscript was handled by A. Bardossy, Editor-in-Chief, with the assistance of Roger Moussa, Associate Editor

Keywords:
River discharge
Palaeohydrology
Dendrochronology
Bayesian regression
Climate variability
Water supply

ABSTRACT

Long-term river discharge records are essential for water resource management, especially in semi-arid regions. However, the short instrumental records in Iran and the limited availability of local paleoclimate proxies to extend these records hinder our understanding of the full range of hydrologic variability. To help overcome these constraints, we have used annually-resolved tree-ring width chronologies from a network of sites spanning the eastern Mediterranean to the Tibetan Plateau to develop the first multi-centennial (~500 years) river discharge reconstruction for the Dez River basin, a catchment that supports substantial water extraction in southwestern Iran. A Hierarchical Bayesian Regression (HBR) model accompanied by parsimonious predictor selection was used to derive the most robust model output. The selection method retained 26 precipitation-sensitive tree-ring width chronologies, mainly from regions with similar hydroclimate features to the Dez River basin. The resulting reconstruction of the most downstream gauging station accounts for 62% of the variance in river discharge observations, closely matching known historical events and other regional reconstructions. Notably, the underlying recurrence pattern of extreme flow conditions suggests floods were more frequent than low flow extremes (i.e., droughts) during much of the 18th and early 19th centuries. In contrast, during the early 17th century, droughts were more frequent. Worryingly, the frequency of both floods and droughts has increased simultaneously since the beginning of the twentieth century. Our reconstruction could be used to assess current water allocation strategies under conditions similar to past extended dry periods. When combined with future projections, they can help provide more robust assessment scenarios for water management.

1. Introduction

The combined effects of increased climate variability and greater demand for water resources have highlighted the importance of sustainable management for many of the world's river basins (Loucks, 2017). Access to quality-controlled hydrologic data, specifically river discharge records, is critical for achieving sustainable management (Stewart, 2015). However, the limited availability and short length of instrumental river discharge observations make it hard to assess long-term variability, directly affecting secure and sustainable water supply management. The development history of the Colorado River and the over-allocation of water resources based on an abnormally wet period (1906–1919) is a widely known example of this kind of problem (Galelli et al., 2021; Meko et al., 2022; Woodhouse and Lukas, 2006a). Data paucity remains a challenge for many parts of the world, especially arid and semi-arid regions like Iran. Additionally, these regions face challenges due to substantial hydroclimatic variability, exacerbated by recent and predicted future anthropogenic climate change (Hobeichi

* Corresponding author.
E-mail address: s.sharifazari@unsw.edu.au (S. Sharifazari).

https://doi.org/10.1016/j.jhydrol.2023.129895
Received 7 June 2022; Received in revised form 18 June 2023; Accepted 28 June 2023
Available online 12 July 2023
0022-1694/© 2023 The Author(s). Published by Elsevier B.V. This is an open access article under the CC BY license (http://creativecommons.org/licenses/by/4.0/).

et al., 2022; Masih et al., 2009; Vaghefi et al., 2019).

Precipitation in Iran is highly variable in both space and time due to seasonal cycles, the country's large size and topographic complexity (Raziei et al., 2012). In recent decades, Iran has faced increased inter-annual variability, with severe drought and flood events dramatically impacting local communities. In 2019 a number of extreme flood events across Iran caused a human disaster and substantial loss of assets and infrastructure. This unprecedented flooding immediately followed a devastating multi-year drought (Alborzi et al., 2022). However, records of climate and river discharge only began with hydropower development in the mid-1950s. This hampers our understanding of recent extreme events, and whether they are unusual in the context of longer-term climate variability.

Despite considerable uncertainty in climate projections, climate change has been identified as contributing to the magnitude and rapid transition between extreme events in Iran (Abbaspour et al., 2009; Rahimi et al., 2019). There is general agreement amongst climate models for increasing temperatures over Iran, but the effect of climate change on future rainfall is highly uncertain, especially over the Zagros Mountains. The lack of long-term and continuous data to appropriately evaluate and contextualise projected future trends in climate models has been recognized as one of the underlying reasons for this uncertainty (Rahimi et al., 2019).

In areas with short hydrologic records, like Iran, stochastic time series methods are commonly used to incorporate climate uncertainty in the water resources design or management plans (Mehrotra and Sharma, 2006). However, stochastic models may not capture river discharge variability on decadal or longer timescales, which are important for future planning. Paleoclimate data, specifically annually resolved tree-ring chronologies, can provide additional information on the range of natural variability over multi-decadal time frames (Meko and Woodhouse, 2011). Annual tree-ring widths (i.e., tree growth) and river discharge share common climatic controlling factors such as winter snowpack, precipitation, and summer temperature (Meko et al., 1995; Woodhouse and Lukas, 2006b). Thus tree-ring-derived records can be valuable proxies (i.e., predictors) for extending river discharge records back in time.

To help understand hydrologic variability in southwestern Iran, we present the first multi-centennial tree-ring reconstruction for the Dez River basin using an Hierarchical Bayesian Regression (HBR) model. HBR models have been increasingly used for river discharge reconstructions (Devineni et al., 2013; Higgins et al., 2022; Rao et al., 2020; Rao et al., 2018). The HBR framework shares common information across river discharge gauges within a basin, reducing uncertainty in the reconstruction by shrinking the number of model parameters. This means HBR models are especially beneficial for river discharge reconstructions in areas with only short instrumental records which are poorly suited to conventional linear regression techniques (Cook et al., 2010; Harley et al., 2017; Meko and Woodhouse, 2011).We then investigate the patterns of low/high flow extremes and how their frequency of occurrence has varied over time and explore whether the recent spate of extreme events is unusual compared to the previous five centuries. Finally, we compare our reconstruction with documented historical flood/dry events and other hydroclimate reconstructions within the region and nearby countries to help validate our reconstruction.

2. Study area and data

2.1. Study area

The geographic extent of the Dez basin stretches from 48°10′ to 50°21′ eastern longitude and from 31°34′ to 34°7′ northern latitude in the southwestern part of Iran. The Dez River is the main tributary of the Karoon River, and joining together, they form the Great Karoon River (also known as the Karun and Karoun). Importantly, the Karoon River is a major source of water for agricultural and economic activity, with the largest withdrawal of any Iranian river system (Ashraf et al., 2019). The Dez River itself consists of two main tributaries, Sezar and Bakhtiyari. This river system originates from the Zagros Mountains and flows towards the Persian Gulf. A sub-basin area of about 16,200 km^2 with an average annual flow of around 7,600 million cubic meters (M m^3) contributes water into the Dez reservoir (3,300 M m^3; shown in Fig. 1b). The Dez Dam enables about 125,000 ha of irrigated agriculture in Khuzestan and provides 520 megawatts of hydropower (Felfelani et al., 2013). The dam has also been proposed as the primary alternative source of drinking water for more than 4.7 million people in the central and southern parts of Khuzestan province (Majedi et al., 2020).

The average elevation of the basin is 1,970 m but ranges from as low as 330 m to 4,150 m at the highest point (Oshtoran Kuh; Fig. 1a). The Köppen-Geiger system has classified a range of climates in the region, from arid with hot and dry summers in the downstream areas to temperate with dry and cold summers in the upstream regions (Beck et al., 2018). The basin receives an average annual precipitation of around 500 mm, while its average potential evapotranspiration is about 1,400 mm per year. Almost all precipitation falls during the wet season extending from November to May, with parts of it as snow during Jan-Mar over the upper regions of the river basin (Meidani and Araghinejad, 2014; Saghafian and Davtalab, 2007). Westerly disturbances, mid-latitude cyclones that originate in the Mediterranean region and move eastward, control the intra-annual variability (Winstanley, 1973, Syed et al., 2010, Arsalani et al., 2021), while large-scale climate drivers such as the El Niño-Southern Oscillation (ENSO) and Pacific Decadal Oscillation (PDO) influence precipitation and river discharge variations on longer timescales (Meidani and Araghinejad, 2014). Fig. 1c shows the climatological basin-average monthly temperature and year-to-year variability in monthly basin-average precipitation.

2.2. River discharge and climate data

Daily river discharge data have been recorded at four hydrometric stations in the Dez River basin since 1955. Compared to other river basins in Iran, the Dez River has a relatively complete record of flow data, and the river had not been significantly impacted by upstream activities until recently (~2008). Daily river discharge data for three upstream gauges, namely Sepid Dasht Sezar (G21-285) at Sezar tributary, Tang Panj Bakhtiyari (G21-293) at Bakhtiyari tributary, and Tale Zang (G21-295) on Dez River were directly sourced from Iran's Water Resources Management Company (IWRMC) database for this study. A few daily values were missing in some years for G21-293 and G21-295, which accounted for<5% of the length of the January-June wet season (i.e., the target season for reconstruction). Therefore, their omission from the annual series was assumed not to have any noticeable impact. Also, the continued period of missing data at G21-293 during 2008–2009 was outside the time period selected for building the reconstruction model. Table 1 summarizes the characteristics of gauges used in this study.

The variability in monthly flows for the gauging stations is shown in Fig. 2 with a map of the river system in the top-left panel. River discharge from January-June accounts for more than 70% of the annual flow, and almost 50% of river discharge occurs during March-May (Fig. 2). River discharge follows the monthly variation seen in precipitation records but with a lag of more than one month. Flows in February and March are mostly direct run-off, while snowmelt accounts for most of the river discharge in April and May (Meidani and Araghinejad, 2014). We used Pearson correlation and a two-sided hypothesis test to evaluate the relationship between ground station observations of monthly climate (precipitation and temperature) and averaged Jan-Jun river discharge (Fig. 3a) and identified the main climate seasons relevant to river discharge in the Dez basin. To evaluate the spatial pattern of this relationship across a wider area that stretches from the eastern Mediterranean to the Tibetan Plateau, we used the CRU TSv4.06 dataset

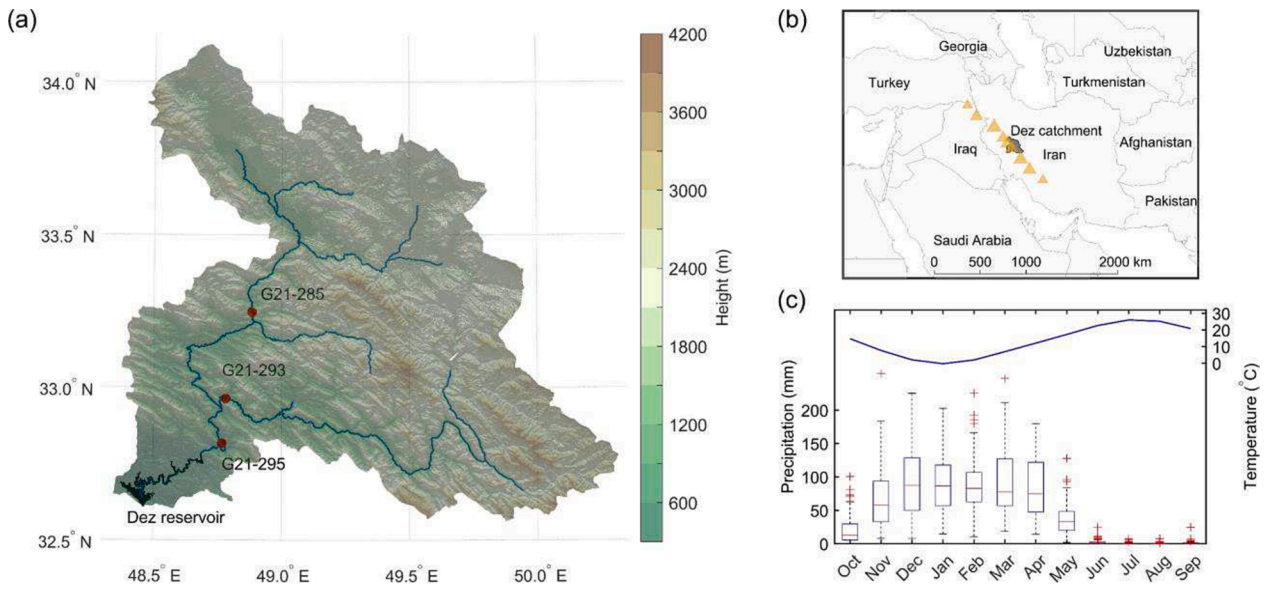

Fig. 1. (a) Topography of the Dez River basin and the locations of the river discharge gauges used in this study (red circles). (b) The position of the basin in the context of Iran and the wider West Asia region is shown on the right, with the orange triangles indicating the Zagros Mountain Range. (c) Boxplots showing monthly basin-average precipitation (mm, left axis) for the period of 1956–2013, with climatological basin-average monthly temperature (°C, right axis) for the same period plotted in blue. (For interpretation of the references to colour in this figure legend, the reader is referred to the web version of this article.)

Table 1
Summary data of the selected flow gauges on the Dez River.

Gauge name	Longitude (°E)	Latitude (°N)	River/Tributary	Basin Area (km^2)	Average annual flow (M m^3)	Data period
Sepid Dasht Sezar	48.88	33.22	Sezar	7,180	1,325	1956–2013
Tang Panj Bakhtiyari	48.77	32.93	Bakhtiyari	6,437	4,307	1956–2013
Tale Zang	48.77	32.82	Dez	16,200	7,610	1956–2013

(Harris et al., 2022). The CRU TS dataset is derived by the interpolation of monthly climate observations with an improvement in the interpolation method for the newer versions (Harris et al., 2020), and its accuracy has been suggested to be acceptable for countries located in the area mentioned above including Iran (Saemian et al., 2021) and Pakistan (Abbas et al., 2022).

2.3. Tree ring data

Few annually resolved local tree-ring chronologies have been developed from broadleaf or conifer climate-sensitive species in the central and southern Zagros Mountains, and only two of them go back to mid-1500 (Arsalani et al., 2021; Arsalani et al., 2018; Azizi et al., 2013). Remote tree-ring sites from the wider region, including Turkey, Pakistan, and other neighbouring countries can also be used for river discharge reconstruction as similar climate drivers affect these countries (Cullen and Demenocal, 2000; Martin-Benito et al., 2016; Rao et al., 2018; Winstanley, 1973). Many long and well-replicated tree-ring chronologies exist from neighbouring countries providing a good source of information for river discharge reconstruction in Iran.

For this study, we identified available tree-ring records from countries neighbouring Iran, mostly within the scale of regional weather systems, defined as within a 2,500 km distance (Boers et al., 2019) from the basin boundary. An initial pool of approximately 380 annual-ring width series from Turkey, Georgia, Jordan, Lebanon, and parts of Greece to the west and Pakistan, Tajikistan, parts of India and a small part of Kyrgyzstan to the east were downloaded from the International Tree Ring Data Bank (ITRDB)(https://www.ncei.noaa.gov/products/paleoclimatology/tree-ring). The raw annual ring-width records were then standardized using the Regional Curve Standardization (RCS) (Briffa et al., 1992) and the signal-free method (Melvin and Briffa, 2008) to remove growth trends thought to be unrelated to climate and to preserve decadal and longer (i.e., medium to low-frequency) climate variation. The chronologies obtained from this process were then used as pool of potential predictors for our river discharge reconstruction model.

3. Methods

3.1. Predictor selection

From the initial pool of available tree-ring width chronologies, only those that extended up to and beyond 2001 were chosen for analysis. The end date of river discharge reconstruction (2001) was selected as a trade-off between a declining pool of chronologies and maximising the length of the overlapping instrumental period for calibration and verification. We also included the one-year lagged tree chronologies (i.e., t + 1) for river discharge predictors, as this year's climate condition may affect tree growth in the following year (Rao et al., 2018). Since river discharge data were positively skewed at all three gauges, discharge was log-transformed to ensure that they were normally distributed (verified using a Kolmogorov-Smirnov test). Chronologies that correlated significantly with log-transformed discharge (Pearson correlation, $p < 0.05$ two-tailed *t*-test) were retained as the final predictors. Correlations of the chronologies were calculated both for the current year and the previous year (i.e., lag 0 and lag 1). To prevent unequal chronology representation in the predictor pool, only the highest correlated chronology was retained at either lag 0 or lag 1. Principal component analysis was used to reduce the dimensionality of the data and hence the number of free parameters to be estimated (Cook et al., 1994). Thus, the principal component (PC) scores were used directly as model predictors rather than the tree-ring width chronologies. Only PCs with eigenvalues greater than one were used as final river discharge predictors following

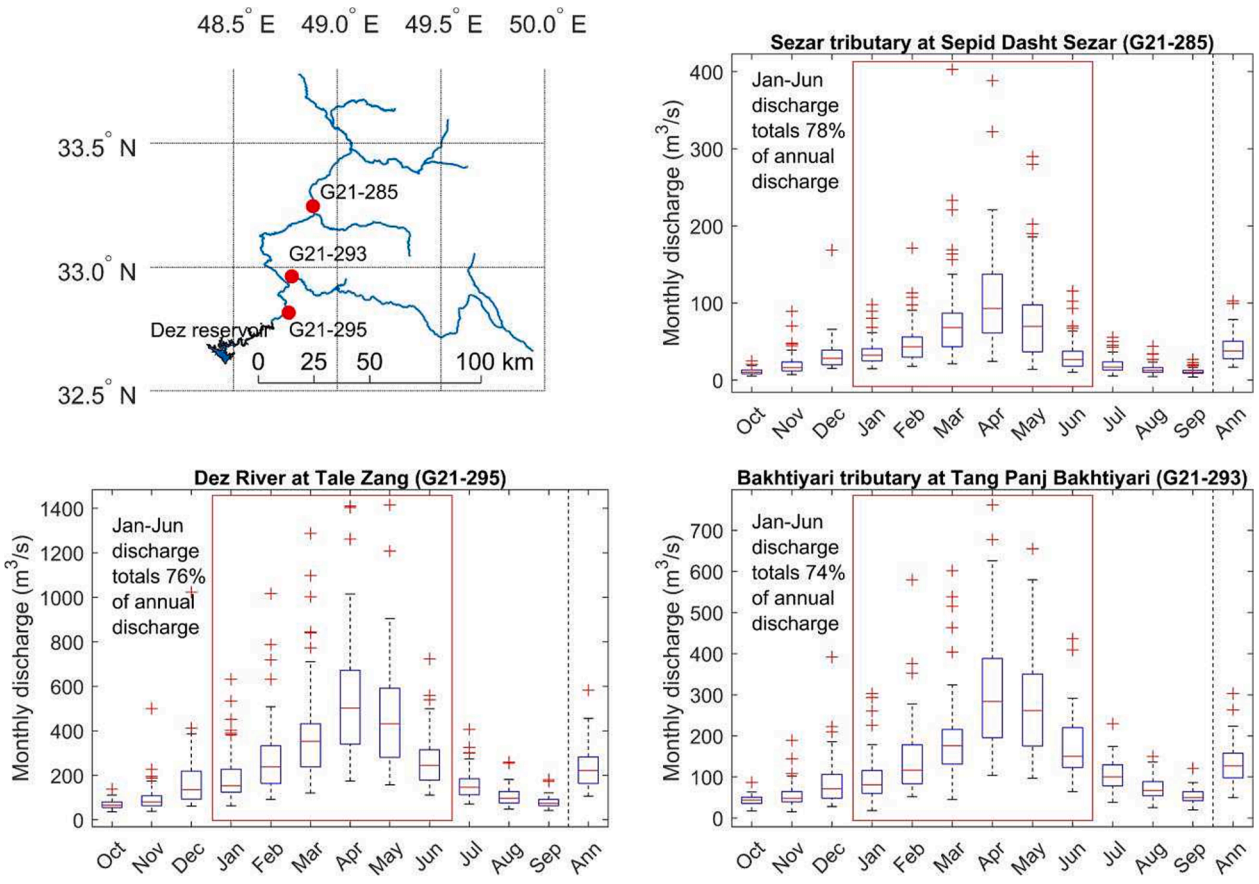

Fig. 2. The location of three river discharge gauges (top-left panel) in the Dez River basin and boxplots showing the associated monthly and annual discharge (m^3/s) over the instrumental period. The red outline in the Boxplots highlights the seasonal window (i.e. January through to June) selected for flow reconstruction. (For interpretation of the references to colour in this figure legend, the reader is referred to the web version of this article.)

the Kaiser–Guttman cutoff criteria as an estimate of common shared signal (versus noise) between the tree ring predictors (Guttman, 1954).

To ensure that the selected predictor locations share relatively similar hydroclimate features with the Dez River basin, we calculated the Knoben-Woods-Free distance (KWF; Knoben et al., 2018) between tree ring locations and the center of the river basin (Nguyen et al., 2020). The KWF is the Euclidean distance in the hydroclimate space characterized by aridity, moisture seasonality, and snow fraction indices at $0.5^\circ \times 0.5^\circ$ resolution. Knoben et al. (2018) sourced climatic data from CRU and river discharge data from Global Runoff Data Centre data archives to calculate these indices. The KWF between the center of the Dez basin and each grid point in the analysis region (10°N-20°E and 50°N-80°E) ranged from 0 to 1.95.

3.2. Reconstruction model

Devineni et al. (2013) demonstrated that sharing common information across river discharge gauges through a Hierarchical Bayesian Regression (HBR) framework reduces the uncertainty in river discharge reconstruction. Such a model was used in this study, and it can be described as follows:

$$y_{i,t}|\alpha_i\beta_i = \alpha_i + \beta_i \times X_t + \varepsilon_{i,t}$$

$$\varepsilon_{i,t} \sim MVN(0, \Sigma_e)$$

$$\beta_i \sim MVN(\mu_\beta, \Sigma_\beta)$$

With non-informative priors modelled as:

$$\alpha_i \sim N(0, 10^4)$$

$$\mu_\beta \sim MVN(0, 10^4 I)$$

$$\Sigma_\beta \sim \text{Inv} - \text{Wishart}_{\nu_0}(\Lambda_0)$$

$$\Sigma_e \sim \text{Inv} - \text{Wishart}_{\nu_1}(\Lambda_1)$$

Where $y_{i,t}$ is the averaged Jan-Jun river discharge recorded at gauge i in year t. X is the matrix of PCs of selected tree ring chronologies. β_i is the vector of regression coefficients for the predictor PCs, α_i is the regression intercept, and $\varepsilon_{i,t}$ is the error term for gauge i in year t. As the river discharge data is highly skewed, we used the log-transformed data for modelling. Following Devineni et al. (2013), the back-transformed reconstruction data, i.e., inverse logarithm of HBR model estimates, were used for evaluating modelling skill. As all flow series are correlated with each other (Figure S1), a common multivariate normal distribution (MVN) was used to model the regression coefficients. Drawing the covariance structure of regression coefficients (β_i) from this MVN allows the pooling of common information across river discharge gauges (Devineni et al., 2013). It also decreases the uncertainty by reducing the number of model parameters. The hierarchical structure of the regression model is constructed by describing the MVN parameters using the hyperparameters of μ_β and Σ_β (Gelman and Hill, 2006). We assumed that the regression error terms could also be correlated across flow gauges by drawing them from a multivariate normal distribution with the covariance matrix of Σ_e.

The priors of Σ_β and Σ_e covariance matrices were taken to be inverse Wishart distributions with scale matrices of Λ_0 and Λ_1, respectively (Devineni et al., 2013). The scale matrices were defined as identity matrices with ν_0 and ν_1 degrees of freedom set to be one more than the number of predictors and one more than the number of gauges,

respectively (Devineni et al., 2013). Following Rao et al. (2018), we estimated the parameters of the joint posterior distribution by employing a Gibbs sampler, a Markov Chain Monte Carlo (MCMC) method, through simulating three chains. A detailed description of the model was provided by Rao et al. (2018) and Devineni et al. (2013).

We used a nested approach in which shorter predictors were sequentially dropped from the predictor pool when going back in time (Meko, 1997). The initial model was based on all the tree-ring predictors and a new regression model was built for each nest using the PCs scores of only the remaining tree-ring chronologies after the shorter series were dropped. No further nest was formed if there were fewer than two significant predictors. We then scaled the variance of reconstruction obtained from each nest to that of the instrumental data over the calibration period and appended the reconstruction of longer nests to the start year of the younger ones to develop the final reconstruction (Rao et al., 2018). The weighted ensemble method developed by (Cook et al., 2010) was also used to produce a series of river discharge reconstructions. The ensemble method explicitly incorporates the covariance between river discharge and the tree-ring series. This was done by multiplying the tree ring predictors by a power of their correlations with the river discharge data during the calibration period before principal component analysis to create each weighted ensemble (i.e. $wTr = Tr \times r^w$, where wTr and Tr are the weighted and unweighted tree-ring series). The weights (w) ranged from 0 to 2 (0.0, 0.1, 0.25, 0.5, 0.67, 1.0, 1.5, 2.0), with higher values giving increasing weight to those predictors most highly correlated with river discharge. Thus, PC scores of the weighted ensemble with higher weights (i.e., more than 0.5) are primarily influenced by tree-ring chronologies with stronger correlations rather than chronologies with weaker correlations. Note that only tree rings with significant correlations at the 5% *level*, i.e., $r = \pm 0.29$ in our case) are included. This method of perturbing predictors to generate the ensemble reconstruction acknowledges that the presence of noise in the data makes it difficult to determine an optimal correlation weight that should be applied to tree-ring predictors when incorporated into the reconstruction model (Cook et al., 2010).

3.3. Model verification

The relatively short overlapping period (1956–2001; 46 years) between tree ring predictors and river discharge data made it hard to implement the conventional split-sample cross-validation method used in tree-ring reconstructions. Thus, we used the moving-block cross-validation approach described by Nguyen et al. (2020) to verify our regression model. This method enables the model to capture any regime shifts (Briffa, 1998) by withholding a contiguous block of data for verification and results in a set of scores useful for providing a robust estimate of the reconstruction skill (Nguyen et al., 2020). The size of the block was the median of the largest significant autocorrelation lag of any chronology in the predictor pool (i.e., 8 years). This meant ~ 17% of data was withheld for verification, and the remainder was used for calibration. This approach resulted in 39 iterations for each weighted PCA and for each nest. In each iteration, the regression model was calibrated on 36 years between 1956 and 2001 and validated on the omitted remaining contiguous block of 8 years. Considering the eight different correlation weights described in section 3.2 meant a total of 312 (39×8) runs were undertaken to derive the final reconstruction and its verification statistics. Following Rao et al. (2020), we used the median of all 312 runs, including both reconstructions and their relevant calibration-verification statistics, as the final reconstruction.

The calibration period coefficient of multiple determination (CRSQ or R^2), the verification period reduction of error (VRE), and the verification period coefficient of efficiency (VCE) defined by (Cook et al., 1999) were used to assess the performance of our reconstructions. VRE evaluates the reconstruction relative to the calibration mean and ranges from $-\infty$ to 1, where values greater than 0 indicate the superiority of the reconstructions over the calibration mean. VCE is equivalent to the Nash-Sutcliffe Coefficient of Efficiency in hydrology (Nguyen et al., 2020), and it is more rigorous than VRE as it measures the performance of reconstructions relative to the verification mean, always resulting in a smaller value compared to VRE unless the calibration and verification means are identical. Thus, VCE and VRE greater than 0 indicates some useful skill in reconstruction (Cook et al., 2010). The two verification values are calculated as follows:

$$VRE = 1 - \left[\frac{\sum (y - \widehat{y}_i)^2}{\sum (y_i - \overline{y}_c)^2}\right]$$

$$VCE = 1 - \left[\frac{\sum (y_i - \widehat{y}_i)^2}{\sum (y_i - \overline{y}_v)^2}\right]$$

Where y_i and $\widehat{y}_i$ are observed and back-transformed reconstructed river discharge, $\overline{y}_c$ is the mean of the actual data in the calibration period, while $\overline{y}_v$ is the mean of the data in the verification period.

3.4. Extreme event analysis

Extreme low flow events were classified as values below the lower 5th percentile of the reconstruction mean (Higgins et al., 2022; Hoang et al., 2016). Similarly, extreme high flows were above the 95th percentile. As the intervals between consecutive extreme low flow or consecutive extreme high flow are not normally distributed (Mudelsee et al., 2004), a non-parametric Gaussian kernel function was used to estimate the changes in the occurrence rates of extreme events. We followed the Sheather and Jones (1991) method to select the bandwidth of the Gaussian kernel function and obtained a 90% confidence band of the occurrence rates using 2,000 bootstrap simulations.

Besides extreme low and high flow events, multi-year dry or wet episodes as well as the frequency of swings from wet to dry and vice-versa, are all important for water resources management, especially in semi-arid regions. Consequently, we identified the number of multi-year dry and wet events in the reconstruction period. A period of three or more years for which all reconstructed flows were smaller than the mean of reconstructions minus half of its standard deviation (σ; sigma) and at least two years of that was one sigma below the mean were recognized as multi-year dry events (Ben-Zvi, 1987). The opposite defined multi-year wet events. For each 30-year moving window, we calculated the transition probability from dry to wet event by dividing the number of dry years (i.e., years with the reconstructed flow below the mean by more than 0.5 sigma (Ho et al., 2017)), which were followed by wet years, by the total number of the dry years within that window. Also, the transition probability from a year with flow higher than the reconstruction mean by more than 0.5 sigma was considered as the probability of swinging from a wet event to a dry one.

4. Results

4.1. Selected tree ring predictors

The predictor selection process retained 26 tree-ring width chronologies for the reconstruction (Table S1). Almost all the final tree-ring width predictors are from locations identified as climatically similar to the Dez basin with a KWF<0.75 (i.e., more climatically similar than the mean KWF calculated for all grids). Fig. 3b shows the locations of the selected tree-ring width predictors plotted on the KWF map.

We also evaluated the relationship between monthly precipitation and temperature and Jan-Jun river discharge at Tale Zang station. As shown in Fig. 3a Jan-Jun river discharge positively correlates with the previous December ($p < 0.05$) and the current year January through April ($p < 0.01$ for February, March, and April) basin precipitation. The seasonal window of December through April accounts for more than 75% of the basin's annual precipitation, and it is highly correlated ($r = 0.84$, $p < 0.001$) with the river discharge series at all three gauges. Very

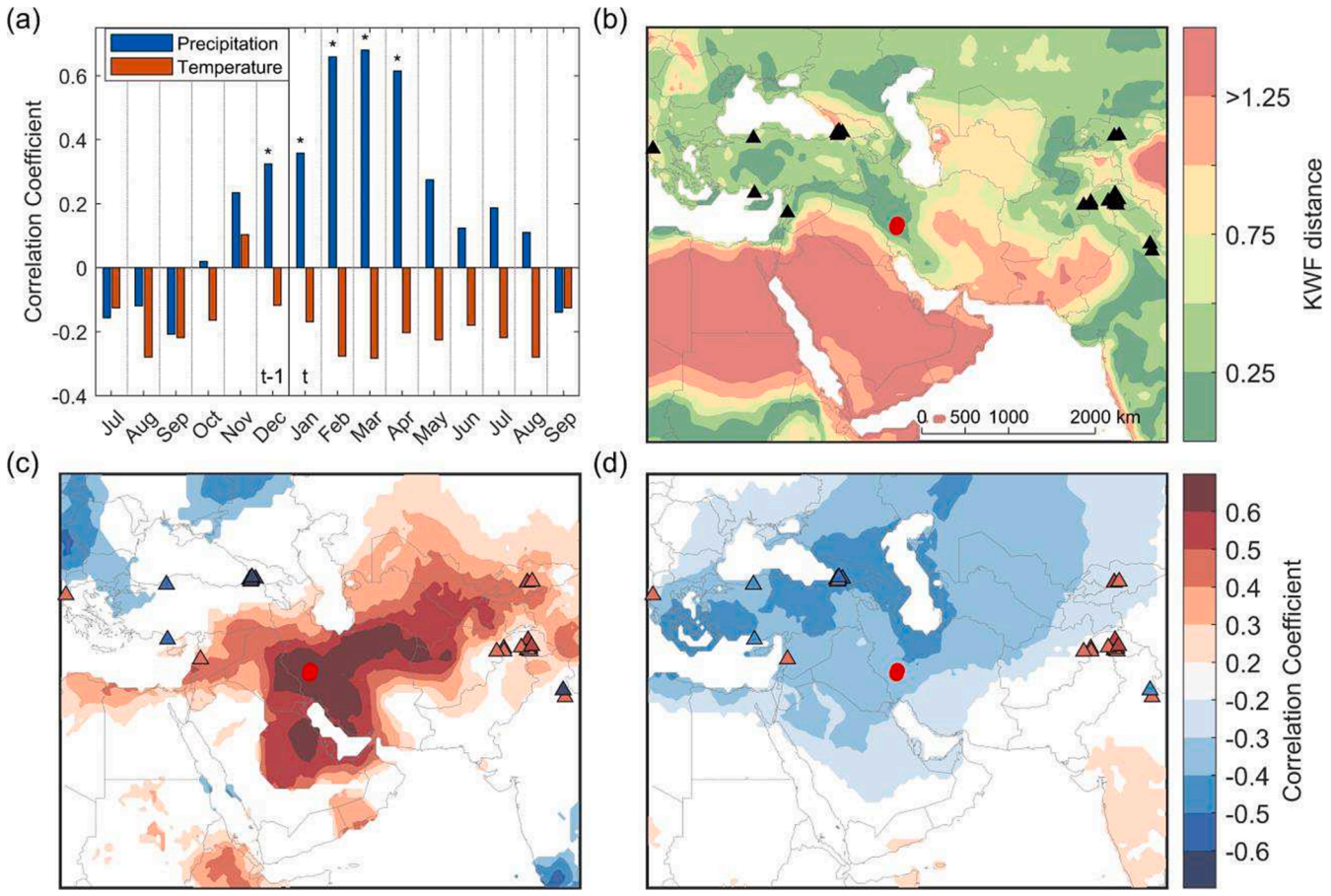

Fig. 3. (a) Pearson correlations between averaged Jan-Jun river discharge (1956–2001) at Tale Zang and month-by-month basin precipitation (blue) and temperature (red; *, $p < 0.05$) for months between prior year (t-1) July and current year (t) September. (b) The KWF distance between the center of the Dez basin and other locations within the geographical region of 10°N-20°E and 50°N-80°E. The black triangles show the locations of 26 tree-ring width chronologies with a significant correlation ($p < 0.05$) to all river discharge gauges used in regression modeling. (c) Spatial Pearson correlation fields ($p < 0.1$) comparing the averaged Jan-Jun river discharge and total Dec-Apr CRU precipitation fields during the period of 1956–2001. Infill shading in triangles show the mean Pearson correlation between averaged Jan-Jun river discharge at all gauges and each tree-ring width predictor. (d) Same as for figure (c) but with averaged Jan-Jun CRU temperature fields. (For interpretation of the references to colour in this figure legend, the reader is referred to the web version of this article.)

low rainfall in the summer months (Fig. 1c) means that these months generally have no significant relationship with river discharge. While temperature is not significantly correlated with river discharge in any single month, average Jan-Jun temperature is negatively correlated ($p < 0.01$, $r = -0.38$) with Jan-Jun river discharge at Tale Zang station. To assess the spatial footprint of the climate-to-discharge relationship, we computed Pearson correlation fields between Dec-Apr precipitation (Fig. 3c) and Jan-Jun temperature (Fig. 3d) with Jan-Jun river discharge. We found that Jan-Jun river discharge at Tale Zang is positively correlated ($p < 0.1$) with Dec-Apr precipitation over a broad region stretching from the Levant to the Karakoram. Applying correlation analyses to other precipitation products, such as datasets from the Global Precipitation Climatology Centre and the fifth generation of atmospheric reanalysis, produced consistent results (Figure S2). Negative correlations ($p < 0.1$) with Jan-Jun temperature were also found with higher latitude areas from Anatolia to the eastern Caspian Sea. The correlation between the selected chronologies and Jan-Jun river discharge is consistent with the broad pattern of previously described temperature-river discharge and precipitation-river discharge correlations.

4.2. River discharge reconstructions

The final averaged Jan-Jun river discharge reconstruction for the Dez River basin from the selected tree ring chronologies spans 1510–2013, with instrumental data appended after 2001 (Fig. 4). The tree-ring width chronologies used in this study explained 50–62% of the variance in river discharge observations at each gauge during the calibration period (1956–2001). Table 2 shows the median skill scores used to evaluate the reconstruction validity for the best-replicated nest (1793–2001) and the whole reconstruction interval (1510–2001).

The reconstructions provide meaningful information for the entire 1510–2001 period; the median of VRE and VCE for the best-replicated nest ranges from 0.25 to 0.47, and the VCE values stayed positive for each flow gauge moving back in time until 1510. The median skill scores for each reconstruction nest from 1510 to 2001, for each of the three river discharge gauges, and the number of tree-ring width chronologies contributing to each reconstruction nest are presented in Table S2. The result for Sepid Dahst Sezar is the weakest of the three gauges as it has the lowest mean Jan-Jun river discharge, and it may be influenced by local conditions more than by broad climate signals captured by the selected chronologies (Nguyen et al., 2020; Strange et al., 2019).

Fig. 4a shows the median of all 312 ensemble members for the most recent, best-replicated nest for the Dez River discharge at the most downstream gauge (Tale Zang, gauge G21-295) compared with the measurements over the instrumental period. As can be seen from Fig. 4a, the median of the reconstructions matches the instrumental flow, capturing both interannual variability and most of the extreme flow events. While some of the peak flows from 1969 to 1976 are underestimated based on the median of reconstructions, they are located

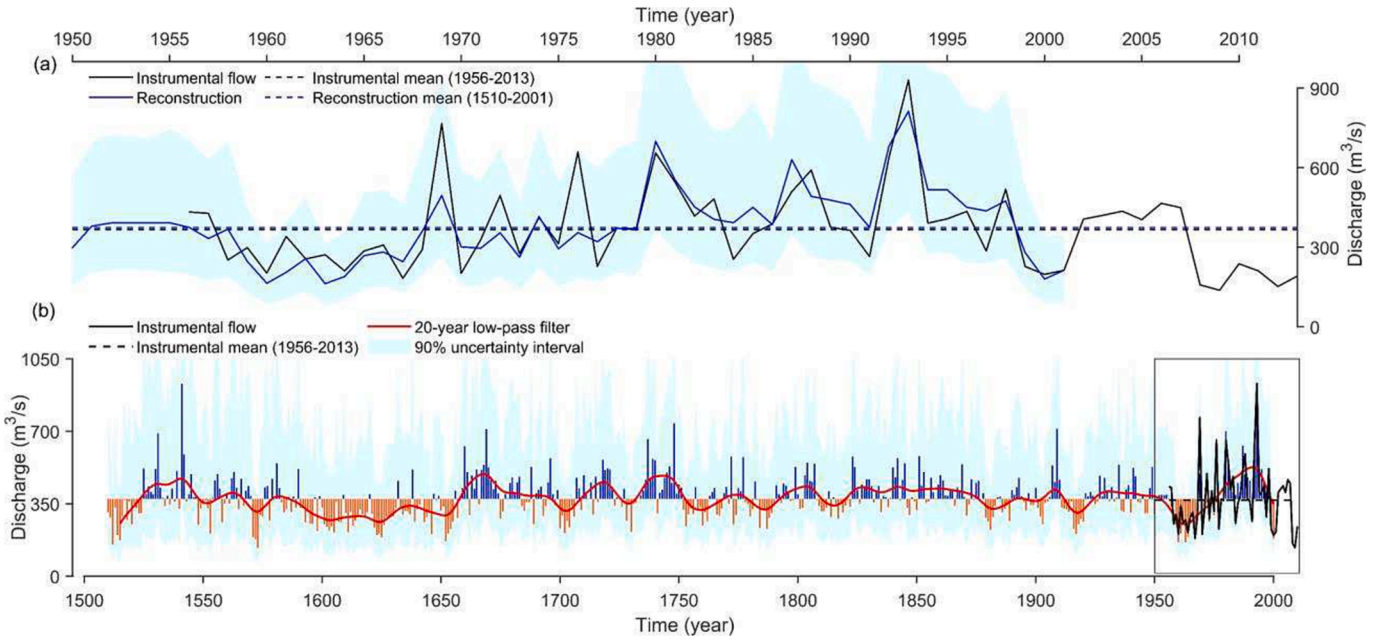

Fig. 4. (a) Instrumental (black) versus reconstructed (blue) average Jan-Jun river discharge in m^3/s for Dez River G21-295 over the instrumental period 1956–2013 with the 90% confidence interval for reconstruction shown in light sky blue. (b) Reconstructed averaged Jan-Jun discharge at G21-295 and its associated 90% confidence interval. Reconstruction values greater than the reconstruction mean are shown in vertical blue lines, and values less than the reconstruction mean are shown in orange. The solid red line shows the 20-year low-pass filtered reconstruction. The box in panel (b) shows the timing of the period included in panel (a). (For interpretation of the references to colour in this figure legend, the reader is referred to the web version of this article.)

Table 2
Reconstruction skill of the HBR model for the three Dez basin gauges. Values are given for the initial nest (1793–2001) and the whole reconstruction interval (1510–2001) (see Section 3.3 for parameter explanations).

		Initial nest (1793–2001)				Median values (1510–2001)			
Gauge name	Gauge number	R^2	R^2_{adj}	VRE	VCE	R^2	R^2_{adj}	VRE	VCE
Sepid Dasht Sezar	G21-285	0.50	0.45	0.41	0.25	0.44	0.39	0.37	0.16
Tang Panj Bakhtiyari	G21-293	0.60	0.57	0.47	0.30	0.55	0.51	0.46	0.24
Tale Zang	G21-295	0.62	0.58	0.47	0.35	0.56	0.52	0.45	0.26

within the range of the 90% confidence interval shown in Fig. 4. The mean of Jan-Jun river discharge at G21-295 during the instrumental period (1956–2013) is slightly lower than the mean over the 1510–2013 reconstruction interval by ~ 2%. However, the period 1598–1655 (equivalent length to the instrumental period) represents the lowest pre-instrumental river discharge and is significantly lower than the reconstruction mean by 22% (two-sided *t*-test $p < 0.01$). Thus, making decisions based on the instrumental flow average alone to manage the growing demands for water within the basin may be risky and result in overallocation in the future. The results for other gauges are similar to G21-295 (Figures S3 and S4).

We used a 30-year sliding window to assess changes in the variance and the transition probability from wet to dry and dry to wet events in the reconstruction period. The largest variance occurred in the late 20th century, and the early 17th century had the lowest variance, a part of a consistent period of low variability occurring from ~ 1750 to ~ 1900. As shown in Fig. 5a, the variance of reconstructed flow for the instrumental period (1956–2001) is unprecedented over the whole reconstruction interval and is significantly greater than the mean reconstruction variance for the period after 1700 (Levene's test, $p < 0.01$). The reconstructed flow of this period accounts for more than 50% of the variance in river discharge observations in almost all three gauges. The transition probability plot in Fig. 5b shows two periods with frequent swings between dry and wet events (1550–1690 and 1625–1785), followed by a long period of almost no transition events until 1925. After this stable period, the probability of rapid shifts between dry and wet events increased again. The transition probability from dry to wet events increased to a maximum after 1930, and from wet to dry events reached its highest after 1950.

We identified multi-year wet/dry events over the reconstruction interval based on the definition given in section 3.4. These events are shown in Fig. 6. The longest multi-year drought event occurred in the early 17th century (1621–1630, 10 years), and the longest multi-year high flow period happened in the instrumental period (1992–1998, 7 years). While the second-longest wet event occurred in the early 18th century (1717–1722, 6 years), the second longest-dry (1959–1967, 9 years) event occurred during the instrumental period and is comparable with its corresponding longest duration event in terms of magnitude. The results in Figs. 5 and 6 demonstrate that the instrumental period has the highest variability over the entire reconstruction interval.

4.3. Recurrence intervals of extremes

A bandwidth of 35 years was selected for the nonparametric Gaussian kernel to analyse the occurrence rate of low and high-flow extreme events. We adopted a value slightly smaller than the estimated value (38 years) by the Sheather and Jones (1991) method as a slight under smoothing allows for easier identification of significant variation (Mudelsee et al., 2003). Fig. 7 shows the occurrence rate curves of the Dez River's low and high flow extremes at G21-295 with a 90% confidence band. Low-flow extreme events were identified as the years for which their corresponding river discharge values were below

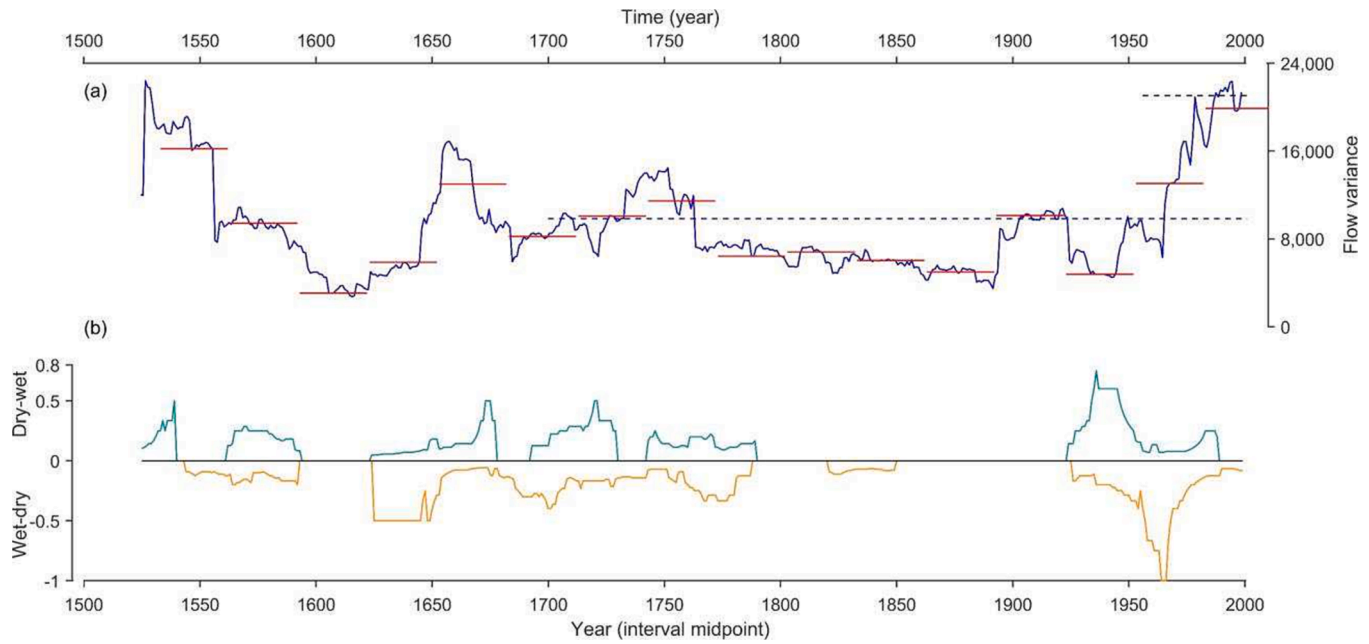

Fig. 5. (a) The variance of the reconstruction is based on a 30-year sliding window (blue) and consecutive non-overlapping 30-year windows (red). Dashed blue and black lines are the variance of Jan-Jun flow at Tale Zang over the 1700–2001 and 1956–2001 periods, respectively. (b) Changes in the transition probability from dry to wet (dark cyan) and wet to dry (dark orange) years are based on the 30-year running period. (For interpretation of the references to colour in this figure legend, the reader is referred to the web version of this article.)

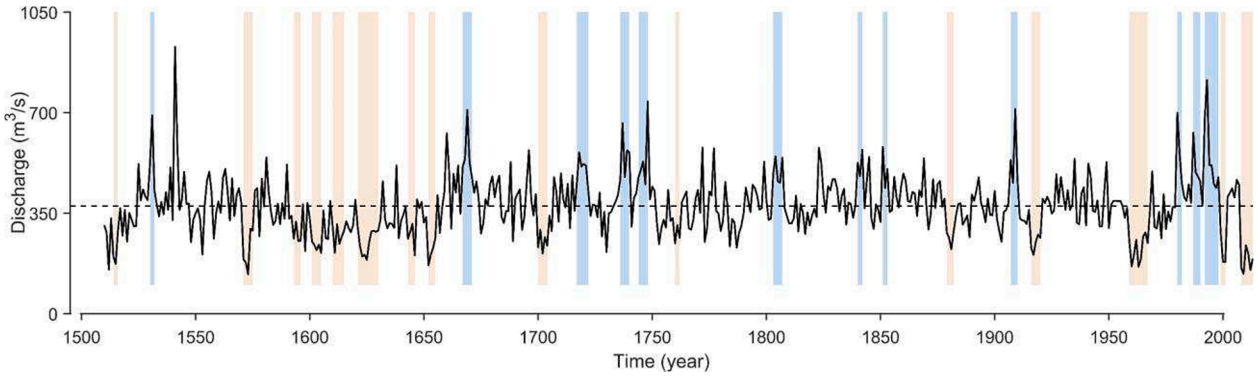

Fig. 6. Reconstructed averaged Jan-Jun discharge for Dez River at Tale Zang (G21-295) with the mean of reconstructions shown in the dashed black line. The orange bounds represent the multi-year dry periods, while the blue ones generally represent wet periods. (For interpretation of the references to colour in this figure legend, the reader is referred to the web version of this article.)

the 5th percentile of reconstructions, shown in vertical orange lines in Fig. 7 (with the opposite case for high-flow extreme events illustrated in blue). Two distinguishable peaks for each low and high flow are evident from their corresponding curves, which are significant based on their bootstrap confidence intervals. The occurrence rate peaked at around 1620 for low flow extremes and at around 1755 for high flow extremes reaching frequencies higher than 10 years. However, secondary peaks in both high and low flow extremes occurred during the instrumental period at around 2000. Changing the end date of reconstruction from 2001 to 2013 and appending the observations to the reconstructions makes the second peak of low flow extremes even more distinguishable (see dashed lines in Fig. 7), indicating a trend towards drier conditions (Mousavi et al., 2019; Norouzi, 2020).

5. Discussion

In addition to the modelling skill metrics, we assessed our reconstruction against documented extreme events such as famines and floods and to other regional climate reconstructions to verify its reliability (Fig. 8). Our reconstruction corresponds to documentary data of Iran's great famines of 1870–1872 (Arsalani et al., 2021; Okazaki, 1986; Seyf, 2010) and 1917–1919 (Foroozan et al., 2020; Majd, 2013), with reconstructed Jan-Jun flows at least half a standard deviation below the reconstruction mean in these years for all gauging stations. Extraordinary winter rains and snowfalls throughout Iran were reported for 1909–1911 (Melville, 1984), with our reconstruction also showing very high Jan-Jun flow for these years. The effect of the Laki eruption (1783–1784) on the region (Gao et al., 2008; Mikhail, 2016) is also evident in our reconstruction, where the reconstructed value for 1784 was more than one sigma below normal and it was followed by a 4-year contiguous period of dry events (1786–1789). The considerable amount of aerosols injected into the atmosphere by the Laki eruption weakened the westerly disturbances in the year of eruption and subsequent years, leading to reduced precipitation in areas from the Middle East to Western Himalayas (Mikhail, 2016; Misra et al., 2021). Additionally, our reconstruction is well-correlated (Pearson correlation, $p < 0.05$ two-tailed *t*-test) with the local Standardized Precipitation Index (SPI) reconstruction (Arsalani et al., 2021) for southwestern Iran, and it is

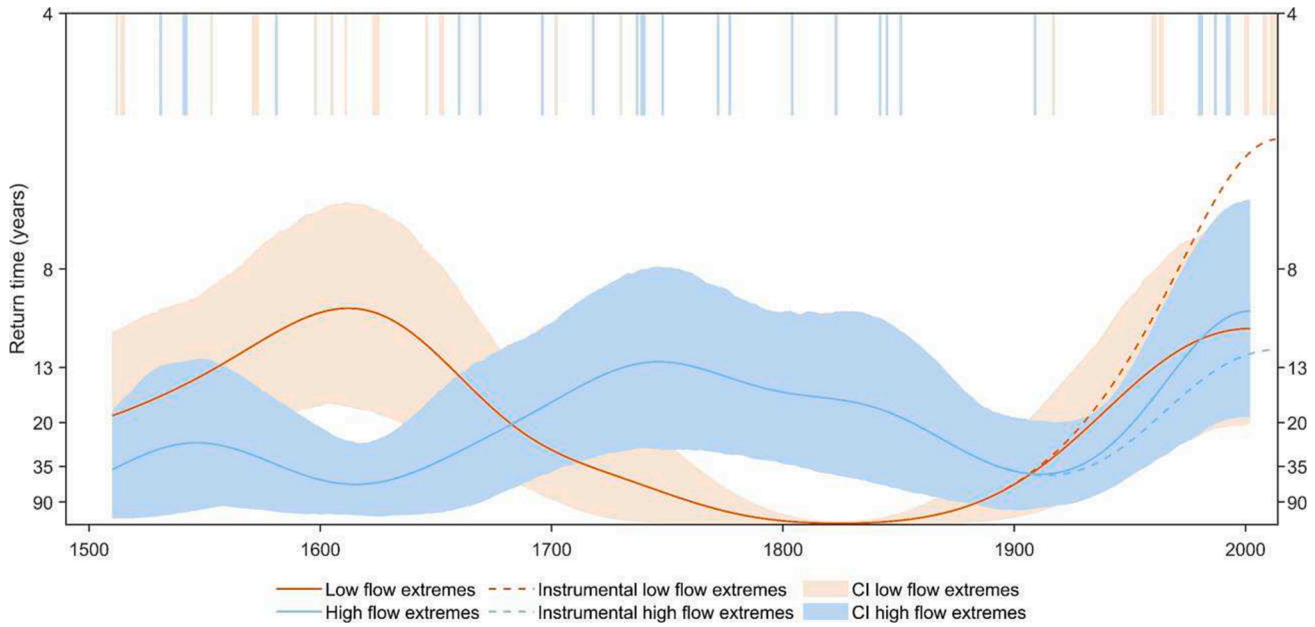

Fig. 7. Extreme high flow and low flow event years and the time-varying frequency of the occurrence (i.e., the return time or average time interval between extreme events) of these events between 1510 and 2001 for Dez River at G21-295, with dashed lines showing the adjusted frequency curve if instrumental data is appended to the reconstruction after 2001. A kernel occurrence rate estimator (Mudelsee et al., 2003, Silva et al., 2012) was used with a bandwidth of 35 years (solid lines). The shaded areas (blue and orange) represent the 90% confidence intervals based on 2,000 bootstrap simulations. (For interpretation of the references to colour in this figure legend, the reader is referred to the web version of this article.)

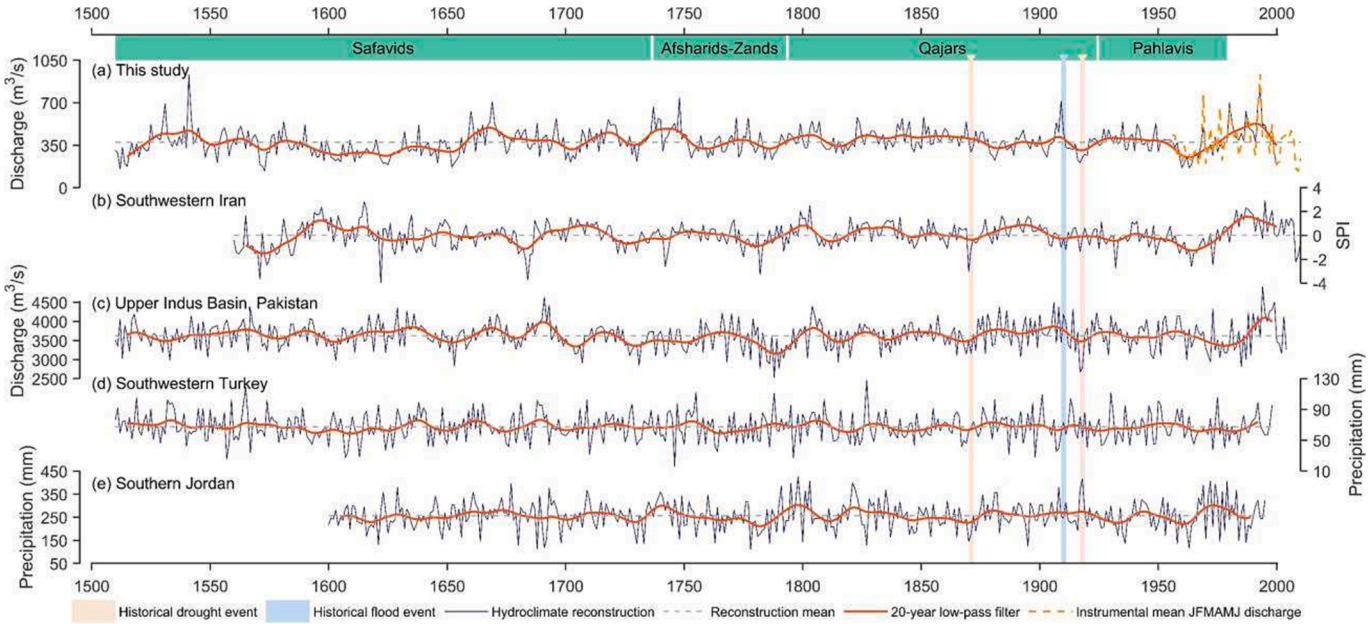

Fig. 8. Comparison of the reconstructed January-June averaged discharge for Dez River at G21-295 (a) with reconstructed October–March SPI in southern Iran (b; Arsalani et al., 2021), reconstructed mean May through September (MJJAS) discharge in the upper Indus Basin (c; Rao et al., 2018), reconstructed May–June precipitation in southwestern Turkey (d; Touchan et al., 2003), and reconstructed October–May precipitation in southern Jordan (e; Touchan et al., 1999). The vertical orange and light blue lines indicate the historical droughts/famines (1870–1872 and 1917–1919) and floods (1909–1911) experienced throughout Iran, including the study area. The solid red lines indicate the 20-year low-pass filtered reconstruction, and the horizontal dashed grey lines show the mean of hydroclimate reconstructions. (For interpretation of the references to colour in this figure legend, the reader is referred to the web version of this article.)

consistent with river discharge reconstructions for Pakistan ($p < 0.1$) (Rao et al., 2018). Also, significant positive correlations ($p < 0.05$) were found between the 20-year low-pass filter of our reconstruction and the corresponding filters of regional precipitation reconstructions for Turkey (Touchan et al., 2003) and Jordan (Touchan et al., 1999) (Fig. 8). All reconstructions are entirely independent except for Rao et al. (2018), in which five chronologies used in our modelling were previously used in their reconstruction, incorporating 25% of their predictors.

The spatial coverage of tree ring predictors used in our reconstruction model stretches from the eastern Mediterranean to the Tibetan Plateau. Westerly disturbances are the primary synoptic system during the wet season in this area (Cannon et al., 2015; Mehterian et al., 2017), and they account for the greatest amount of annual precipitation over

Iran (Alijani and Harman, 1985). Thus, selecting tree ring chronologies from eastern and western parts of this area provides information about climate signals common to the whole area, which is helpful for river discharge reconstruction in southwestern Iran. Therefore, our reconstruction supports the suggestion of Arsalani et al. (2021) for using their developed chronologies from southwestern Iran for hydroclimate reconstruction in surrounding countries.

We observe a high frequency of low flow extremes from the late 16th to the early 18th centuries, broadly corresponding to the Little Ice Age (LIA; Grove (2019)). Drier than average conditions in the Middle East and Eastern Mediterranean during the LIA are supported by paleolimnological evidence (Roberts et al., 2012) and coral records (Felis et al., 2018) and included the Eastern Mediterranean great drought of 1591–1596 CE (White, 2013). A decreasing trend in the reconstructed Jan-Jun river discharge can be observed beginning from the 1670s, leading to a severe megadrought drought in the early 18th century (1700–1704). Gustafson and Speer (2022) argue that the environmental crisis mostly resulted from droughts that started in the late 17th century and contributed to the collapse of the Safavids empire. Regional SPI reconstruction from local tree-ring chronologies by Arsalani et al. (2021) also showed high frequencies of extreme dry events, expressed by SPI $<$ -2, and long dry phases during the 16th, 17th, and 18th centuries.

While these dry conditions seemed to continue until the mid-19th century in the Middle East (Felis et al., 2018) and southwestern Iran (Arsalani et al., 2021), we find that high-flow events were more frequent during the 1730s to 1860s in our reconstructions compared to the preceding two centuries. Many severely cold winters and flooding events have been reported in historical records for our study area and its nearby provinces during this period (Melville, 1984). In agreement with our findings, the 18th century was also identified as the wettest period over the last 500 years in a tree-ring reconstruction for northern Iran's precipitation (Foroozan et al., 2020).

Unlike the late 16th to mid-19th periods, the twentieth century was a period of high frequencies of both low-flow and high-flow extremes (Fig. 7). Since the mid-twentieth century, both multi-year low flow extremes and multi-year high flow extremes occurred frequently, and there are frequent swings between dry and wet events. This finding is consistent with the local SPI reconstruction (Arsalani et al., 2021), in which the 20th century was the period with the highest frequency of both extreme dry and wet events. It also supports the recently recognized shift in the operation of the Earth system from the mid-20th that led to the variability exceeding its natural range (Ripple et al., 2019; Turney and Fogwill, 2021) and the detected increase in severe hydroclimatic events since then for South America (Morales et al., 2020). Changes in extremes and increasing trends in drought severity and flood magnitude from the 1970s have been detected in Iran from precipitation observations and river discharge records across the country (Modarres et al., 2016). The observed climate data also shows that the transition from one extreme to another has been accompanied by the intensification in the magnitude of extremes in recent years (Dezfuli, 2020). For example, the last two decades mostly consisted of extended drought episodes (Ghamghami and Irannejad, 2019), but many major floods, initiated by intermittent heavy rainfalls, have occurred in Iran since the beginning of the century (Madani, 2014; Vaghefi et al., 2019), making the water year wetter than normal and contributing to the greatest portion of inflow to reservoirs.

The increasing variability and transitions between droughts and floods lead to more uncertainty, which has important implications for water resources management. As an example, during prolonged drought in the region, decisions made during the early months of the subsequent water year may be biased towards conservation policies affecting flood-control activities if that year turns out to become extremely wet. For the multi-purpose Dez reservoir, it is argued that inadequate flood controls by reservoir operators during the 2019 flood, affected by the preceding drought conditions that prioritized storing water for the agricultural sector, contributed to the severe damage to the downstream areas (Zarei et al., 2021). Although this recent variability has been captured in the instrumental record, putting it in a centuries-long context shows that recent dry episodes and discharge reduction (Mousavi et al., 2019; Norouzi, 2020) could plausibly last as long as those experienced in the early 17th. Thus, the reconstruction provides valuable insights into the possible variability of water availability and may help to develop effective allocation strategies for agricultural water supply in the semi-arid downstream area of Dez dam. A better understanding of the range of natural variability of water availability in arid regions where the agricultural sector faces growing conflict between water supply and demand under climate change (Peng et al., 2023) contributes to provide certainty on future infrastructure needs and planning and more effective water resources management.

Although our river discharge reconstruction, in conjunction with other local and regional hydroclimate reconstructions, demonstrates increased variability for the instrumental period, uncertainty remains regarding the extent of hydroclimate variability experienced in the region during previous centuries. The presence of local chronologies in the area underscores the potential for developing a network of tree-ring sites that may involve multiple species and various chronologies, such as tree-ring isotope series. Such a network would enhance the ability to capture the complete spectrum of local-scale climate variability, reducing the likelihood of under- or over-estimation of extreme events. The collection of sites along an elevational gradient would help reveal possible changes in climatic signals with elevation as noted in the neighbouring Himalayan mountain range (Esper et al., 2007). The results of such a study could then be incorporated into investigating the impact of altitude differentiation in the Dez river basin on river discharge variability (Chen et al., 2023). Thus, given its verification against local proxies, our reconstructions could be incorporated into water system models to test the reliability of allocation policies under a wider range of dry and wet conditions experienced in the past. Finally, it could even be combined with observations and future projections to broaden the assessment scenarios for water management plans (Quinn et al., 2020).

6. Conclusions

While long-term river discharge records are essential for water resources management, the maximum length of flow series in Iran rarely exceeds 50 years. Here, we provided the first multi-centennial (~500 years) river discharge reconstructions for southwestern Iran, for the Dez River basin, using annually resolved tree ring chronologies from neighbouring countries. The reconstruction skill, together with its comparison against local SPI reconstructions, regional hydroclimate and river discharge reconstructions, and documented famines/floods showed that it contains valuable information about river discharge variability over the last five centuries in southwestern Iran. Using the most parsimonious predictor selection method and the HBR model, we isolated climate signals in common between river discharge gauges and tree site locations to produce a reliable reconstruction. While our reconstruction is specific to the Dez River, our analysis indicates that the findings are relevant for a much broader region than Southwest Iran. However, there is potential to further improve the reconstruction by including the few local chronologies not currently available through ITRDB and through the development of new local chronologies.

The reconstruction shows that the region has experienced longer megadroughts in the past than have occurred during the instrumental period. However, while low flow extremes were found to be more frequent from the early 16th to early-18th compared to the instrumental period, and high flow extremes peaked at around the mid-18th century, we find that the period since the mid-twentieth century has the overall highest frequency of extreme events (dry and wet extremes occurring in the same period), with increased variance and rapid transitions between hydroclimate extremes. Together, these lines of evidence suggest that increasing variability and decreasing reliability in the flow over the last

70 years are anomalous when compared to the last 500 years. The reason behind this change in annual flow characteristics is not entirely understood, but the rapid transition from one extreme to another has been identified as a potential impact of climate change. These findings have important implications for water resources management which should consider both conservation and flood-controlling policies in decision-making.

7. Data availability statement

All tree-ring chronologies included in the modelling are publicly available from the NOAA/World Data Service for Paleoclimatology archives at https://www.ncei.noaa.gov. The code underpinning this paper and river discharge data are available on request from the corresponding author.

CRediT authorship contribution statement

S. Sharifazari: Conceptualization, Data curation, Formal analysis, Methodology, Visualization, Writing – original draft, Writing – review & editing. **J.G. Palmer:** Data curation, Methodology, Writing – review & editing. **P.A. Higgins:** Methodology, Software, Writing – review & editing. **M.P. Rao:** Software, Writing – review & editing. **F. Johnson:** Supervision, Writing – review & editing. **C.S.M. Turney:** Supervision, Writing – review & editing. **D. Martín-Benito:** Writing – review & editing. **M.S. Andersen:** Supervision, Writing – review & editing.

Declaration of Competing Interest

The authors declare that they have no known competing financial interests or personal relationships that could have appeared to influence the work reported in this paper.

Data availability

Data will be made available on request.

Acknowledgments

The authors acknowledge the efforts of all the dendrochronologists who have contributed tree-ring chronologies to the ITRDB, allowing for studies such as this one to be undertaken. We thank the editor and anonymous reviewers whose comments have improved this manuscript. Australian Government Research Training Scholarships and the UNSW Scientia PhD Scholarship Schemes support SSH and PAH. MPR is supported by a European Union Horizon 2020 Marie Skłodowska-Curie Grant #101031748 and NOAA Climate and Global Change Fellowship under UCAR CPAESS award #NA18NWS4620043B. The UNSW Scientia Program supports FJ. DMB was funded by project RYC-2017-23389 from the Spanish Ministry of Science and Innovation MCIN/AEI. The University of New South Wales facilitated open-access publishing as part of the ScienceDirect (Elsevier) - University of New South Wales agreement via the Council of Australian University Librarians.

Appendix A. Supplementary data

Supplementary data to this article can be found online at https://doi.org/10.1016/j.jhydrol.2023.129895.

References

Abbas, A., Ullah, S., Ullah, W., Waseem, M., Dou, X., Zhao, C., Karim, A., Zhu, J., Hagan, D.F.T., Bhatti, A.S., Ali, G., 2022. Evaluation and projection of precipitation in Pakistan using the Coupled Model Intercomparison Project Phase 6 model simulations. Int. J. Climatol. 42 (13), 6665–6684.

Abbaspour, K.C., Faramarzi, M., Ghasemi, S.S., Yang, H., 2009. Assessing the impact of climate change on water resources in Iran. Water Resour. Res. 45 (10) https://doi.org/10.1029/2008WR007615.

Alborzi, A., Zhao, Y., Nazemi, A., Mirchi, A., Mallakpour, I., Moftakhari, H., Ashraf, S., Izadi, R., AghaKouchak, A., 2022. The tale of three floods: From extreme events and cascades of highs to anthropogenic floods. Weather Clim. Extremes 38, 100495.

Alijani, B., Harman, J.R., 1985. Synoptic Climatology of Precipitation in Iran. Ann. Assoc. Am. Geogr. 75 (3), 404–416. https://doi.org/10.1111/j.1467-8306.1985.tb00075.x.

Arsalani, M., Pourtahmasi, K., Azizi, G., Bräuning, A., Mohammadi, H., 2018. Tree-ring based December–February precipitation reconstruction in the southern Zagros Mountains, Iran. Dendrochronologia 49, 45–56. https://doi.org/10.1016/j.dendro.2018.03.002.

Arsalani, M., Grießinger, J., Pourtahmasi, K., Bräuning, A., 2021. Multi-centennial reconstruction of drought events in South-Western Iran using tree rings of Mediterranean cypress (Cupressus sempervirens L.). Palaeogeogr. Palaeoclimatol. Palaeoecol. 567, 110296 https://doi.org/10.1016/j.palaeo.2021.110296.

Ashraf, S., AghaKouchak, A., Nazemi, A., Mirchi, A., Sadegh, M., Moftakhari, H.R., Hassanzadeh, E., Miao, C.-Y., Madani, K., Mousavi Baygi, M., Anjileli, H., Arab, D.R., Norouzi, H., Mazdiyasni, O., Azarderakhsh, M., Alborzi, A., Tourian, M.J., Mehran, A., Farahmand, A., Mallakpour, I., 2019. Compounding effects of human activities and climatic changes on surface water availability in Iran. Clim. Change 152 (3-4), 379–391.

Azizi, G., Arsalani, M., Bräuning, A., Moghimi, E., 2013. Precipitation variations in the central Zagros Mountains (Iran) since A.D. 1840 based on oak tree rings. Palaeogeogr. Palaeoclimatol. Palaeoecol. 386, 96–103. https://doi.org/10.1016/j.palaeo.2013.05.009.

Beck, H.E., Zimmermann, N.E., McVicar, T.R., Vergopolan, N., Berg, A., Wood, E.F., 2018. Present and future Köppen-Geiger climate classification maps at 1-km resolution. Sci. Data 5 (1), 180214. https://doi.org/10.1038/sdata.2018.214.

Ben-Zvi, A., 1987. Indices of hydrological drought in Israel. J. Hydrol. 92 (1), 179–191. https://doi.org/10.1016/0022-1694(87)90095-3.

Boers, N., Goswami, B., Rheinwalt, A., Bookhagen, B., Hoskins, B., Kurths, J., 2019. Complex networks reveal global pattern of extreme-rainfall teleconnections. Nature 566 (7744), 373–377.

Briffa, K.R., 1998. Trees tell of past climates: but are they speaking less clearly today? Philos Trans R Soc Lond B Biol Sci 353 (1365), 65–73. https://doi.org/10.1098/rstb.1998.0191.

Briffa, K.R., Jones, P.D., Bartholin, T.S., Eckstein, D., Schweingruber, F.H., Karlén, W., Zetterberg, P., Eronen, M., 1992. Fennoscandian summers from ad 500: temperature changes on short and long timescales. Clim. Dyn. 7 (3), 111–119.

Cannon, F., Carvalho, L.M.V., Jones, C., Bookhagen, B., 2015. Multi-annual variations in winter westerly disturbance activity affecting the Himalaya. Clim. Dyn. 44 (1), 441–455. https://doi.org/10.1007/s00382-014-2248-8.

Chen, J., Zhang, J., Peng, J., Zou, L., Fan, Y., Yang, F., Hu, Z., 2023. Alp-valley and elevation effects on the reference evapotranspiration and the dominant climate controls in Red River Basin, China: Insights from geographical differentiation. J. Hydrol. 620, 129397.

Cook, E.R., et al., 2010. Asian Monsoon Failure and Megadrought During the Last Millennium. Science 328 (5977), 486–489. https://doi.org/10.1126/science.1185188.

Cook, E.R., Briffa, K.R., Jones, P.D., 1994. Spatial regression methods in dendroclimatology: A review and comparison of two techniques. Int. J. Climatol. 14 (4), 379–402. https://doi.org/10.1002/joc.3370140404.

Cook, E.R., Meko, D.M., Stahle, D.W., Cleaveland, M.K., 1999. Drought Reconstructions for the Continental United States*. J. Clim. 12 (4), 1145–1162. https://doi.org/10.1175/1520-0442(1999)012<1145:Drftcu>2.0.Co;2.

Cullen, H.M., Demenocal, P.B., 2000. North Atlantic influence on Tigris-Euphrates streamflow. Int. J. Climatol. 20 (8), 853–863.

Devineni, N., Lall, U., Pederson, N., Cook, E., 2013. A Tree-Ring-Based Reconstruction of Delaware River Basin Streamflow Using Hierarchical Bayesian Regression. J. Clim. 26 (12), 4357–4374. https://doi.org/10.1175/JCLI-D-11-00675.1.

Dezfuli, A., 2020. Rare Atmospheric River Caused Record Floods across the Middle East. Bull. Am. Meteorol. Soc. 101 (4), E394–E400. https://doi.org/10.1175/BAMS-D-19-0247.1.

Esper, J., Frank, D.C., Wilson, R.J.S., Büntgen, U., Treydte, K., 2007. Uniform growth trends among central Asian low- and high-elevation juniper tree sites. Trees 21 (2), 141–150. https://doi.org/10.1007/s00468-006-0104-0.

Felfelani, F., Movahed, A.J., Zarghami, M., 2013. Simulating hedging rules for effective reservoir operation by using system dynamics: a case study of Dez Reservoir, Iran. Lake Reserv. Manage. 29 (2), 126–140. https://doi.org/10.1080/10402381.2013.801542.

Felis, T., Ionita, M., Rimbu, N., Lohmann, G., Kölling, M., 2018. Mild and Arid Climate in the Eastern Sahara-Arabian Desert During the Late Little Ice Age. Geophys. Res. Lett. 45 (14), 7112–7119. https://doi.org/10.1029/2018GL078617.

Foroozan, Z., Grießinger, J., Pourtahmasi, K., Bräuning, A., 2020. 501 Years of Spring Precipitation History for the Semi-Arid Northern Iran Derived from Tree-Ring δ18O Data. Atmos. 11 (9), 889.

Galelli, S., Nguyen, H.T.T., Turner, S.W.D., Buckley, B.M., 2021. Time to Use Dendrohydrological Data in Water Resources Management? J. Water Resour. Plan. Manag. 147 (8), 01821001. https://doi.org/10.1061/(ASCE)WR.1943-5452.0001422.

Gao, C., Robock, A., Ammann, C., 2008. Volcanic forcing of climate over the past 1500 years: An improved ice core-based index for climate models. J. Geophys. Res. Atmos. 113 (D23) https://doi.org/10.1029/2008JD010239.

Gelman, A., Hill, J. (Eds.), 2006. Data Analysis Using Regression and Multilevel/Hierarchical Models. Cambridge University Press.
Ghamghami, M., Irannejad, P., 2019. An analysis of droughts in Iran during 1988–2017. SN Applied Sciences 1 (10), 1217. https://doi.org/10.1007/s42452-019-1258-x.
Grove, J.M., 2019. Little ice ages: ancient and modern. Routledge.
Gustafson, J., Speer, J., 2022. Environmental Crises at the End of Safavid History: The Collapse of Iran's Early Modern Imperial Ecology, 1666–1722. Int. J. Middle East Stud. 54 (1), 57–79.
Guttman, L., 1954. Some necessary conditions for common-factor analysis. Psychometrika 19 (2), 149–161.
Harley, G.L., Maxwell, J.T., Larson, E., Grissino-Mayer, H.D., Henderson, J., Huffman, J., 2017. Suwannee River flow variability 1550–2005 CE reconstructed from a multispecies tree-ring network. J. Hydrol. 544, 438–451.
Harris, I.C., Jones, P., Osborn, T., 2022. CRU TS4.06: Climatic Research Unit (CRU) Time-Series (TS) version 4.06 of high-resolution gridded data of month-by-month variation in climate. Centre for Environmental Data Analysis.
Harris, I., Osborn, T.J., Jones, P., Lister, D., 2020. Version 4 of the CRU TS monthly high-resolution gridded multivariate climate dataset. Sci. Data 7 (1), 109. https://doi.org/10.1038/s41597-020-0453-3.
Higgins, P.A., Palmer, J.G., Rao, M.P., Andersen, M.S., Turney, C.S.M., Johnson, F., 2022. Unprecedented High Northern Australian Streamflow Linked to an Intensification of the Indo-Australian Monsoon. Water Resour. Res. 58 (3) https://doi.org/10.1029/2021WR030881.
Ho, M., Lall, U., Sun, X., Cook, E.R., 2017. Multiscale temporal variability and regional patterns in 555 years of conterminous U.S. streamflow. Water Resour. Res. 53 (4), 3047–3066. https://doi.org/10.1002/2016WR019632.
Hoang, L.P., Lauri, H., Kummu, M., Koponen, J., van Vliet, M.T.H., Supit, I., Leemans, R., Kabat, P., Ludwig, F., 2016. Mekong River flow and hydrological extremes under climate change. Hydrol. Earth Syst. Sci. 20 (7), 3027–3041.
Hobeichi, S., Abramowitz, G., Ukkola, A.M., De Kauwe, M., Pitman, A., Evans, J.P., Beck, H., 2022. Reconciling historical changes in the hydrological cycle over land. npj Climate and Atmospheric. Science 5 (1). https://doi.org/10.1038/s41612-022-00240-y.
Knoben, W.J.M., Woods, R.A., Freer, J.E., 2018. A Quantitative Hydrological Climate Classification Evaluated With Independent Streamflow Data. Water Resour. Res. 54 (7), 5088–5109. https://doi.org/10.1029/2018WR022913.
Loucks, D.P., 2017. Managing water as a critical component of a changing world. Water Resour. Manag. 31 (10), 2905–2916.
Madani, K., 2014. Water management in Iran: what is causing the looming crisis? J. Environ. Stud. Sci. 4 (4), 315–328. https://doi.org/10.1007/s13412-014-0182-z.
Majd, M.G., 2013. The Great Famine & Genocide in Iran: 1917-1919. University Press of America.
Majedi, H., Fathian, H., Nikbakht-Shahbazi, A., Zohrabi, N., 2020. Integrated surface and groundwater resources allocation simulation to evaluate effective factors on greenhouse gases production. Water Supply 20 (2), 652–666.
Martin-Benito, D., Ummenhofer, C.C., Köse, N., Güner, H.T., Pederson, N., 2016. Tree-ring reconstructed May–June precipitation in the Caucasus since 1752 CE. Clim. Dyn. 47 (9), 3011–3027.
Masih, I., Ahmad, M.-u.-D., Uhlenbrook, S., Turral, H., Karimi, P., 2009. Analysing streamflow variability and water allocation for sustainable management of water resources in the semi-arid Karkheh river basin. Iran. Physics and Chemistry of the Earth, Parts A/B/C 34 (4-5), 329–340.
Mehrotra, R., Sharma, A., 2006. Conditional resampling of hydrologic time series using multiple predictor variables: A K-nearest neighbour approach. Adv. Water Resour. 29 (7), 987–999. https://doi.org/10.1016/j.advwatres.2005.08.007.
Mehterian, S., Pourmand, A., Sharifi, A., Lahijani, H.A.K., Naderi, M., Swart, P.K., 2017. Speleothem records of glacial/interglacial climate from Iran forewarn of future Water Availability in the interior of the Middle East. Quat. Sci. Rev. 164, 187–198.
Meidani, E., Araghinejad, S., 2014. Long-Lead Streamflow Forecasting in the Southwest of Iran by Sea Surface Temperature of the Mediterranean Sea. Journal of Hydrologic Engineering 19 (8), 05014005. https://doi.org/10.1061/(ASCE)HE.1943-5584.0000965.
Meko, D., 1997. Dendroclimatic reconstruction with time varying predictor subsets of tree indices. J. Clim. 10 (4), 687–696.
Meko, D., Stockton, C.W., Boggess, W.R., 1995. THE TREE-RING RECORD OF SEVERE SUSTAINED DROUGHT1. JAWRA Journal of the American Water Resources Association 31 (5), 789–801. https://doi.org/10.1111/j.1752-1688.1995.tb03401.x.
Meko, D.M., Woodhouse, C.A., 2011. Application of streamflow reconstruction to water resources management. Dendroclimatology. Springer 231–261.
Meko, D.M., Woodhouse, C.A., Winitsky, A.G., 2022. Tree-Ring Perspectives on the Colorado River: Looking Back and Moving Forward. JAWRA. J. Am. Water Resour. Assoc. n/a(n/a), 1–18. https://doi.org/10.1111/1752-1688.12989.
Melville, C., 1984. Meteorological hazards and disasters in Iran: a preliminary survey to 1950. Iran 22 (1), 113–150.
Melvin, T.M., Briffa, K.R., 2008. A "signal-free" approach to dendroclimatic standardisation. Dendrochronologia 26 (2), 71–86. https://doi.org/10.1016/j.dendro.2007.12.001.
Mikhail, A., 2016. Climate and the chronology of Iranian history. Iran. Stud. 49 (6), 963–972.
Misra, K.G., Singh, V., Yadava, A.K., Misra, S., Maurya, R.S., Vishwakarma, S., 2021. Himalayan Blue Pine Deduced Precipitation Record from Cold Arid Lahaul-Spiti, Himachal Pradesh, India. Frontiers in Earth Science 9. https://doi.org/10.3389/feart.2021.645959.
Modarres, R., Sarhadi, A., Burn, D.H., 2016. Changes of extreme drought and flood events in Iran. Global Planet. Change 144, 67–81. https://doi.org/10.1016/j.gloplacha.2016.07.008.
Morales, M.S., Cook, E.R., Barichivich, J., Christie, D.A., Villalba, R., LeQuesne, C., Srur, A.M., Ferrero, M.E., González-Reyes, Á., Couvreux, F., Matskovsky, V., Aravena, J.C., Lara, A., Mundo, I.A., Rojas, F., Prieto, M.R., Smerdon, J.E., Bianchi, L.O., Masiokas, M.H., Urrutia-Jalabert, R., Rodriguez-Catón, M., Muñoz, A. A., Rojas-Badilla, M., Alvarez, C., Lopez, L., Luckman, B.H., Lister, D., Harris, I., Jones, P.D., Williams, A.P., Velazquez, G., Aliste, D., Aguilera-Betti, I., Marcotti, E., Flores, F., Muñoz, T., Cuq, E., Boninsegna, J.A., 2020. Six hundred years of South American tree rings reveal an increase in severe hydroclimatic events since mid-20th century. Proc. Natl. Acad. Sci. 117 (29), 16816–16823.
Mousavi, R.S., Marofi, S., Gupta, H.V., Ahmadizadeh, M., 2019. Statistical Analysis of Discharge Fluctuations in a Semiarid Basin Using Effective Atmospheric Teleconnections: Dez River Basin in Iran. J. Hydrol. Eng. 24 (7), 05019012. https://doi.org/10.1061/(ASCE)HE.1943-5584.0001773.
Mudelsee, M., Börngen, M., Tetzlaff, G., Grünewald, U., 2003. No upward trends in the occurrence of extreme floods in central Europe. Nature 425 (6954), 166–169.
Mudelsee, M., Börngen, M., Tetzlaff, G., Grünewald, U., 2004. Extreme floods in central Europe over the past 500 years: Role of cyclone pathway "Zugstrasse Vb". J. Geophys. Res. Atmos. 109 (D23) https://doi.org/10.1029/2004JD005034.
Nguyen, H.T.T., Turner, S.W.D., Buckley, B.M., Galelli, S., 2020. Coherent Streamflow Variability in Monsoon Asia Over the Past Eight Centuries—Links to Oceanic Drivers. Water Resour. Res. 56 (12) https://doi.org/10.1029/2020WR027883.
Norouzi, N., 2020. Climate change impacts on the water flow to the reservoir of the Dez Dam basin. Water Cycle 1, 113–120. https://doi.org/10.1016/j.watcyc.2020.08.001.
Okazaki, S., 1986. The great Persian famine of 1870–71. Bull. Sch. Orient. Afr. Stud. 49 (1), 183–192.
Peng, J., et al., 2023. The conflicts of agricultural water supply and demand under climate change in a typical arid land watershed of Central Asia. J. Hydrol.: Reg. Stud. 47, 101384 https://doi.org/10.1016/j.ejrh.2023.101384.
Quinn, J.D., Hadjimichael, A., Reed, P.M., Steinschneider, S., 2020. Can Exploratory Modeling of Water Scarcity Vulnerabilities and Robustness Be Scenario Neutral? Earth's. Future 8 (11). https://doi.org/10.1029/2020EF001650.
Rahimi, J., Malekian, A., Khalili, A., 2019. Climate change impacts in Iran: assessing our current knowledge. Theor. Appl. Climatol. 135 (1), 545–564.
Rao, M.P., et al., 2018. Six Centuries of Upper Indus Basin Streamflow Variability and Its Climatic Drivers. Water Resour. Res. 54 (8), 5687–5701. https://doi.org/10.1029/2018WR023080.
Rao, M.P., et al., 2020. Seven centuries of reconstructed Brahmaputra River discharge demonstrate underestimated high discharge and flood hazard frequency. Nat. Commun. 11 (1), 6017. https://doi.org/10.1038/s41467-020-19795-6.
Raziei, T., Mofidi, A., Santos, J.A., Bordi, I., 2012. Spatial patterns and regimes of daily precipitation in Iran in relation to large-scale atmospheric circulation. Int. J. Climatol. 32 (8), 1226–1237. https://doi.org/10.1002/joc.2347.
Ripple, W., et al., 2019. World scientists' warning of a climate emergency. Bioscience.
Roberts, N., et al., 2012. Palaeolimnological evidence for an east–west climate see-saw in the Mediterranean since AD 900. Global Planet. Change 84–85, 23–34. https://doi.org/10.1016/j.gloplacha.2011.11.002.
Saemian, P., et al., 2021. Comprehensive evaluation of precipitation datasets over Iran. J. Hydrol. 603, 127054 https://doi.org/10.1016/j.jhydrol.2021.127054.
Saghafian, B., Davtalab, R., 2007. Mapping snow characteristics based on snow observation probability. Int. J. Climatol. 27 (10), 1277–1286.
Seyf, A., 2010. Iran and the Great Famine, 1870–72. Middle East. Stud. 46 (2), 289–306.
Sheather, S.J., Jones, M.C., 1991. A reliable data-based bandwidth selection method for kernel density estimation. J. Roy. Stat. Soc.: Ser. B (Methodol.) 53 (3), 683–690.
Stewart, B., 2015. Measuring what we manage–the importance of hydrological data to water resources management. Proc. Int. Assoc. Hydrol. Sci. 366, 80–85.
Strange, B.M., et al., 2019. Comparing three approaches to reconstructing streamflow using tree rings in the Wabash River basin in the Midwestern, US. J. Hydrol. 573, 829–840. https://doi.org/10.1016/j.jhydrol.2019.03.057.
Syed, F.S., Giorgi, F., Pal, J.S., Keay, K., 2010. Regional climate model simulation of winter climate over Central–Southwest Asia, with emphasis on NAO and ENSO effects. Int. J. Climatol. 30 (2), 220–235. https://doi.org/10.1002/joc.1887.
Touchan, R., et al., 2003. Preliminary reconstructions of spring precipitation in southwestern Turkey from tree-ring width. Int. J. Climatol. 23 (2), 157–171.
Touchan, R., Meko, D., Hughes, M.K., 1999. A 396-year reconstruction of precipitation In Southern Jordan 1. JAWRA J. Am. Water Resour. Assoc. 35 (1), 49–59.
Turney, C., Fogwill, C., 2021. The implications of the recently recognized mid-20th century shift in the Earth system. Anthropocene Rev. 2053019621995526.
Vaghefi, S.A., et al., 2019. The future of extreme climate in Iran. Sci. Rep. 9 (1), 1464. https://doi.org/10.1038/s41598-018-38071-8.
White, S., 2013. The Little Ice Age Crisis of the Ottoman Empire: A Conjuncture in Middle East Environmental History. Water on sand, Environmental histories of the Middle East and North Africa, pp. 71–90.
Winstanley, D., 1973. Recent Rainfall Trends in Africa, the Middle East and India. Nature 243 (5408), 464–465. https://doi.org/10.1038/243464a0.
Woodhouse, C., Lukas, J., 2006a. Drought, tree rings and water resource management in Colorado. Can. Water Resourc. J. 31 (4), 297–310.
Woodhouse, C.A., Lukas, J.J., 2006b. Multi-Century Tree-Ring Reconstructions of Colorado Streamflow for Water Resource Planning. Clim. Change 78 (2), 293–315. https://doi.org/10.1007/s10584-006-9055-0.
Zarei, M., et al., 2021. Machine-learning algorithms for forecast-informed reservoir operation (FIRO) to reduce flood damages. Sci. Rep. 11 (1), 24295. https://doi.org/10.1038/s41598-021-03699-6.